# Structures of Normal Single-Stranded DNA and Deoxyribo-3′-*S*-phosphorothiolates Bound to the 3′-5′ Exonucleolytic Active Site of DNA Polymerase I from *Escherichia coli*[†,‡]

Chad A. Brautigam,[§] Sengen Sun,[||] Joseph A. Piccirilli,[||] and Thomas A. Steitz*[,⊥]

*Department of Molecular Biophysics & Biochemistry, Department of Chemistry, and Howard Hughes Medical Institute, Yale University, 266 Whitney Avenue, New Haven, Connecticut 06520-8114, and Department of Biochemistry & Molecular Biology, Department of Chemistry, and Howard Hughes Medical Institute, The University of Chicago, 5841 South Maryland Avenue, MC1028, Chicago, Illinois 60637*

*Received June 29, 1998; Revised Manuscript Received October 16, 1998*

ABSTRACT: The interaction of a divalent metal ion with a leaving 3′ oxygen is a central component of several proposed mechanisms of phosphoryl transfer. In support of this are recent kinetic studies showing that thiophilic metal ions (e.g., $Mn^{2+}$) stimulate the hydrolysis of compounds in which sulfur takes the place of the leaving oxygen. To examine the structural basis of this phenomenon, we have solved four crystal structures of single-stranded DNA's containing either oxygen or sulfur at a 3′-bridging position bound in conjunction with various metal ions at the 3′-5′ exonucleolytic active site of the Klenow fragment (KF) of DNA polymerase I from *Escherichia coli*. Two structures of normal ssDNA bound to KF in the presence of $Zn^{2+}$ and $Mn^{2+}$ or $Zn^{2+}$ alone were refined at 2.6- and 2.25-Å resolution, respectively. They serve as standards for comparison with other $Mn^{2+}$- and $Zn^{2+}$-containing structures. In these cases, $Mn^{2+}$ and $Zn^{2+}$ bind at metal ion site B in a nearly identical position to $Mg^{2+}$ (Brautigam and Steitz (1998) *J. Mol. Biol. 277*, 363−377). Two structures of KF bound to a deoxyoligonucleotide that contained a 3′-bridging sulfur at the scissile phosphate were refined at 2.03-Å resolution. Although the bridging sulfur compounds bind in a manner very similar to that of the normal oligonucleotides, the presence of the sulfur changes the metal ion binding properties of the active site such that $Mn^{2+}$ and $Zn^{2+}$ are observed at metal ion site B, but $Mg^{2+}$ is not. It therefore appears that the ability of the bridging sulfur compounds to exclude nonthiophilic metal ions from metal ion site B explains the low activity of KF exonuclease on these substrates in the presence of $Mg^{2+}$ (Curley et al. (1997) *J. Am. Chem. Soc. 119*, 12691−12692) and that the 3′-bridging atom of the substrate is influencing the binding of metal ion B prior to catalysis.

The 3′-5′ exonuclease of the large fragment (or the Klenow fragment, KF[1]) of DNA polymerase I from *Escherichia coli* is postulated to catalyze the hydrolysis of a phosphodiester bond with the aid of two metal ions (*1*, *2*; see Figure 1). One of these divalent cations, metal ion "A", is proposed to help bind and orient both the single-stranded DNA substrate and an attacking water whose p$K_a$ it lowers. The second cation, metal ion "B", plays the crucial role of acting as a Lewis acid to stabilize the negative charge that becomes resident on the leaving 3′ oxygen. Both metal ions are positioned to stabilize the putative pentacovalent transition state. This mechanism (or a similar one) has also been proposed for other phosphoryl transfer enzymes, such as DNA polymerase (*3*−*6*), alkaline phosphatase (*7*), RNase H (*8*), and ribozymes (*1*, *2*, *9*). That metal ion B is essential for this proofreading reaction has been demonstrated by biochemical and X-ray crystallographic means (*10*): a KF 3′-5′ exonuclease (KF exo) mutant which cannot bind metal ion B is also deficient in nuclease activity. The indispensability of metal ion B probably is due to the absence of a general acid in the active site which may donate a proton to the leaving 3′ oxyanion.

Recently, to evaluate the interaction of metal ions with the leaving atom in this and other phosphoryl transfer reactions, DNA analogues known as deoxyribo-3′-*S*-phosphorothiolates (3′PS, see Figure 2a) have been synthesized and their substrate properties studied (*11*−*15*). These compounds possess a sulfur instead of an oxygen at the 3′ leaving position. The action of KF exo on such a substrate has been

[†] This research was supported by NIH Grant GM-22778 to T.A.S.

[‡] Coordinates for the newly determined structures presented in this paper have been deposited in the PDB. See Table 1 for accession numbers.

* Corresponding author.

[§] Department of Molecular Biophysics & Biochemistry, Yale University.

[||] The University of Chicago.

[⊥] Yale University.

[1] Abbreviations: PIPES, piperazine-*N*,*N*′-bis(2-ethanesulfonic acid); MES, 2-(morpholino)ethanesulfonic acid; CCD, charge-coupled device; rms, root-mean-square; KF, the Klenow fragment of DNA polymerase I from *Escherichia coli*; KF exo, the 3′-5′ exonuclease of KF; ssDNA, single-stranded DNA; dUsG, a heptamer deoxyoligonucleotide whose 3′-most phosphodiester linkage contains a 3′-bridging sulfur; exo, exonuclease; all-oxygen-Mg, the KF structure containing normal oligonucleotide, $Zn^{2+}$, and $Mg^{2+}$; all-oxygen-Mn, the KF structure containing normal oligonucleotide, $Zn^{2+}$, and $Mn^{2+}$; dUsG−Mn, the KF structure containing dUsG, $Zn^{2+}$, and $Mn^{2+}$; dUsG−Zn, the KF structure containing dUsG and $Zn^{2+}$; 3′PS, a deoxyribonucleotide containing a deoxyribo-3′-*S*-phosphorothiolate linkage.

10.1021/bi981537g CCC: $18.00 
Published on Web 12/22/1998

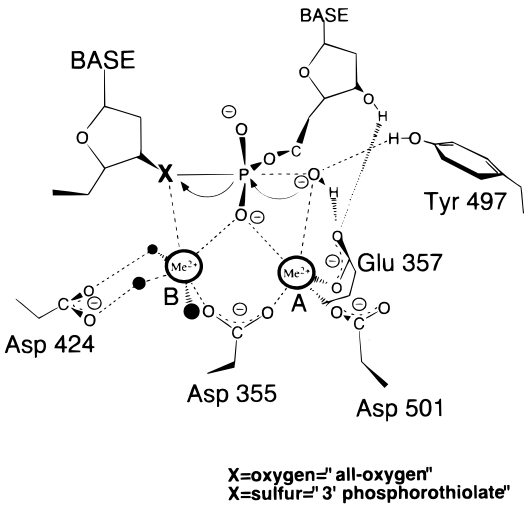


FIGURE 1: Proposed two-metal-ion mechanism for KF 3′-5′ exonuclease for the reactions studied. An activated hydroxide (or water molecule) attacks, having been oriented in the active site by metal ion A and several protein residues. This attack forms the pentacoordinated transition state, which is stabilized by both metal ions. Negative charge builds on the leaving 3′ atom, which is an oxygen normally. This charge is stabilized by metal ion B. The black filled-in circles are water molecules that contact metal ion B. Adapted from ref *37*.

kinetically characterized by Piccirilli and co-workers (*15*; see Figure 2b). In the presence of $Mg^{2+}$, the catalytic efficiency of KF exo on a 3′PS is depressed about 50 000-fold relative to the normal, or "all-oxygen", substrate under identical conditions. However, with $Mn^{2+}$ as the cation, the enzyme is inhibited only about 600-fold. Given the above results and the fact that $S^-$ readily acts as a ligand to $Mn^{2+}$ but not to $Mg^{2+}$ (*16*, *17*), it was concluded that a metal ion plays a vital role in stabilizing the negative charge on the leaving atom. These results are similar to those obtained for the *Tetrahymena* group I intron (*13*, *18*) and the human spliceosomal complex (*19*), where the analogous leaving oxygen atom was substituted by sulfur and the "thio effect" was much relieved by adding thiophilic metal ions to the reaction mixture.

Crystallographic investigations of DNA and metal ions bound to KF exo have proved essential to the understanding of the two-metal-ion mechanism (*1*, *2*, *10*, *20*). Such studies have shown that three acidic side chains in the active site form inner-sphere contacts to the two catalytic metal ions, which are both contacting the pro-$S_p$ oxygen of the scissile phosphate of the substrate, and that metal ion B is well-positioned to promote the formation of the pentacoordinated transition state and to stabilize the developing charge on the leaving atom. In addition, the structures of altered DNA's ($R_p$ and $S_p$ phosphorothioates) bound at the active site of KF exo have been established with a high degree of accuracy at 2.1−2.3-Å resolution (*20*). The extent of structural perturbation that altered substrates induce in the active site correlates well with the in vitro activity of the enzyme on these compounds (*20*−*22*).

The present study uses X-ray crystallography to examine the structural effects that the binding of a 3′PS has on the active site of KF exo in the presence of different metal ions. First, the structures of KF complexed with unmodified substrates in the presence of either $Zn^{2+}/Mn^{2+}$ or $Zn^{2+}$ only were determined at a resolution of 2.6 and 2.25 Å, respectively, to serve as bases for comparison with the 3′PS-containing structures. In these two structures, the substrates bind almost identically, metal ion site A is occupied by $Zn^{2+}$, and metal ion site B harbors either $Mn^{2+}$ or $Zn^{2+}$. Both structures are very similar to a previously reported structure that features $Mg^{2+}$ at metal ion site B (*20*). Next, two structures of KF exo bound to a 3′PS in the presence of either $Zn^{2+}/Mg^{2+}$ or $Zn^{2+}/Mn^{2+}$ were determined at a resolution of 2.03 Å. The 3′PS substrate binds similarly to the normal

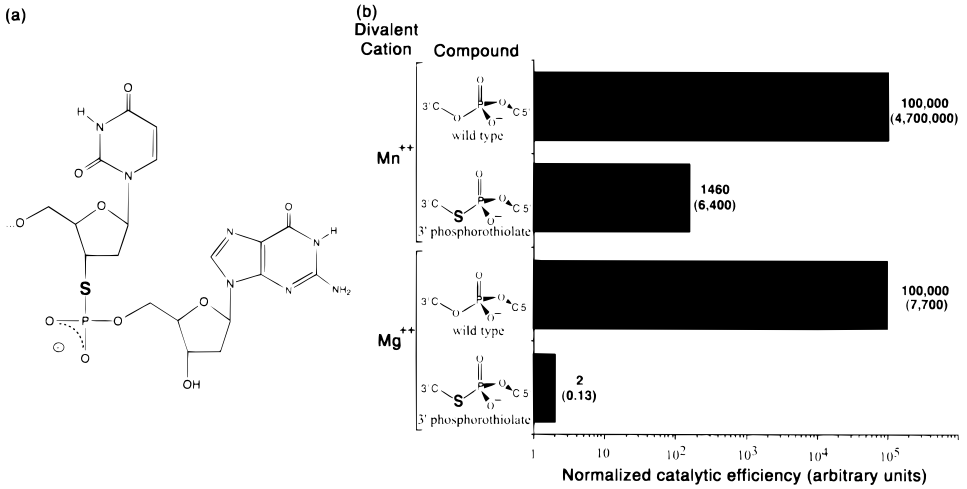


FIGURE 2: Structure and kinetics of 3′ phosphorothiolates. (a) The structure of dUsG, a heptamer deoxyoligonucleotide containing a 3′ phosphorothiolate linkage. Only the final two nucleotides of the heptamer are shown. The only differences between this and a normal DNA oligomer are the presence of the bridging sulfur atom (in bold) and the inclusion of uracil (for synthetic convenience). (b) The effect of 3′ phosphorothiolates on the catalytic efficiency of KF exo. Shown at the far left of the figure is the identity of the cation used. To the right of that, the compound used in each assay is shown, with two possibilities: either the normal all-oxygen oligomer or the 3′ phosphorothiolate (the scissile phosphate of the single-stranded heptamer used is depicted). The horizontal bars show the relative catalytic efficiency of KF exo in the presence of the given combination of substrate and cation. To aid this graphical comparison, the numbers have been normalized such that the catalytic efficiency of KF exo for the all-oxygen heptamer is given the arbitrary value of 100 000. The numbers to the right of each bar show the numerical value associated with each combination, with the value of $K_{cat}/K_M$ before normalization appearing in parentheses, and having units of inverse molar seconds. Note that the scale is logarithmic. Also, it is noteworthy that KF exo is much more efficient in the presence of $Mn^{2+}$ than in that of $Mg^{2+}$. Adapted from ref *15*.

substrates in both of these latter structures. However, binding of this substrate at the active site appears to perturb the binding of both metal ions. In particular, with a 3′PS present, metal ion site B may bind $Mn^{2+}$ or $Zn^{2+}$ but not $Mg^{2+}$. This indicates that the observed diminution of KF exo enzyme activity on a 3′PS in the presence of $Mg^{2+}$ probably is due to substrate-induced disruption of $Mg^{2+}$ binding. This mechanism of inhibition may extend to other systems in which bridging sulfur compounds have been used to explore metal ion interactions with the leaving atom (*13*, *18*, *19*). The present study also illustrates how the 3′-bridging atom of the substrate influences the binding of metal ion B and suggests that $Zn^{2+}$ is likely to support the hydrolysis of a 3′PS by KF exo.

## MATERIALS AND METHODS

*Materials*. The wild-type Klenow fragment was provided by Catherine Joyce. The dUsG deoxyoligonucleotide (sequence: 5′-GCTTAUsG-3′, where "s" stands for the bridging 3′ sulfur atom, see Figure 2a) was synthesized as previously described (*14*, *19*). The deoxyoligonucleotides used for the all-oxygen-Mn study (sequence: 5′-CGTTACGC-3′) and for the all-oxygen-Zn study (sequence: 5′-GCTTACG-3′) were purchased from the Keck Biotechnology Center at Yale and purified as previously described (*20*). All other salts, chemicals, and buffers were purchased from Sigma Chemical Corp.

*Crystal Growth, Storage, Soaking, and Freezing*. KF crystals of space group $P4_3$ and approximate unit cell dimensions of $a = b = 102$ Å and $c = 86$ Å were grown using the vapor diffusion method, under conditions previously described (*20*, *23*). After growth, they were stored in a solution of 2.8 M ammonium sulfate and 50 mM PIPES at pH 7.0. Soaking experiments were carried out in a solution containing 2.8 M ammonium sulfate, 100 mM MES at pH 5.5, 20 mM $MgSO_4$ (or $MnSO_4$), 1 mM $ZnSO_4$, and 1 mM dUsG heptamer. This soak was performed for 1 h, after which the crystals were transferred to a cryostabilization buffer, which consisted of 2.8 M ammonium sulfate, 100 mM MES at pH 5.5, 20 mM $MgSO_4$ (or $MnSO_4$), 1 mM $ZnSO_4$, 16% sucrose (w/v), 8% xylitol (w/v), and 4% glycerol (v/v). The crystals were cryostabilized for 5 min, then supported on a loop of nylon, and plunged into liquid propane. Crystals were stored in solid propane under liquid nitrogen. For the $Zn^{2+}$-only experiment, the $MgSO_4$ or $MnSO_4$ was excluded from the soaking and cryoprotection steps.

*Data Collection, Processing, and Refinement*. The intensity data used for refinement were collected on an Area Detector Systems Corp. CCD detector at CHESS beamline A1 (*24*) and a MAR imaging plate detector at Brookhaven National Laboratories beamline X25. Control data sets were collected on an *R*-axis IV imaging plate system (Molecular Structure Corp.). All data were collected at 100 K. Intensities were processed, scaled, and merged using the HKL suite of programs (*25*). Initial phases were calculated from a high-resolution structure of KF (Jäger, J., and Steitz, T. A., unpublished), but nonisomorphism between this structure and the data collected for these studies necessitated the rigid-body refinement of the model into the current data sets using X-PLOR (*26*). This allowed the modeling of substrates and metal ions into $\sigma_A$-weighted (*27*) electron-density maps using the program O (*28*). Electron density was not present for the entire deoxyoligonucleotide in any of the structures. For the unmodified substrates, the 3′-terminal dinucleotide was modeled into electron density, and the 3′-terminal trinucleotide was modeled for the bridging sulfur substrates. Refinement then proceeded using iterative rounds of positional refinement, individual *B*-factor refinement, and water placement using X-PLOR and O. A bulk-solvent correction was applied to the data at all steps after the rigid-body refinement, which allowed the low-resolution data to 20 Å to be used. The $Zn^{2+}$ anomalous differences were not measured using the standard inverse-beam protocol. Instead, the Friedel mates were separated from one another in the inherently redundant data sets using SCALEPACK. All anomalous-difference density maps were calculated using the CCP4 suite of programs (*29*). Statistics concerning data collection and refinement are given in Table 1.

## RESULTS

*All-Oxygen-Mn Structure*. The 2.6-Å resolution structure of KF exo complexed to a normal, single-stranded DNA oligonucleotide in the presence of $Zn^{2+}$ and $Mn^{2+}$ (the "all-oxygen-Mn structure") has been solved and refined to an *R* factor of 19.8% and an $R_{free}$ of 24.2% in order to provide a basis for comparison with other structures containing manganese. Because crystalline KF exo can hydrolyze oligonucleotides (*30*), certain measures had to be taken to prevent this (*20*). Hydrolysis was averted in all of the experiments in this study by soaking the substrate and metal ions into KF crystals at an inhibitory pH for short times (pH 5.5, 1 h), followed by freeze-trapping the resulting complexes at approximately 85 K. In addition, the X-ray diffraction data were collected at cryogenic temperatures (100−110 K). The all-oxygen-Mn structure shows that, as with the previously determined $Zn^{2+}/Mg^{2+}$-all-oxygen structure (the "all-oxygen-Mg structure"; *20*), two metal ions bind in conjunction with substrate DNA at the active site in the presence of $Mn^{2+}$ and $Zn^{2+}$ (Figures 3 and 4a). The identity of these cations has been ascertained using an anomalous-difference electron-density map (Figure 4b). Because only $Zn^{2+}$ has a significant anomalous signal at the wavelength at which these data were collected (0.908 Å), any peaks in such a map are directly attributable to the presence of $Zn^{2+}$ at that position. This analysis shows that metal ion A is a zinc ion. This metal ion has inner-sphere contacts to Asp 355, Glu 357, Asp 501, and the pro-*S* oxygen of the scissile phosphate of the substrate (parts a and b of Figure 4). Metal ion B has been assigned as a $Mn^{2+}$, because it exhibits no signal in the anomalous-difference density map. The manganese ion is quite disordered, refining to a *B* factor of about 71 Å$^2$. Perhaps owing to this disorder or more likely to the lower resolution of this structure, only a single water molecule is observed in inner-sphere contact with metal ion B, in contrast to the three water molecules encountered in the all-oxygen-Mg structure.

*Comparison of the All-Oxygen-Mn and All-Oxygen-Mg Structures*. Superposition of the structure described above with the all-oxygen-Mg structure (*20*) shows only very small differences (Figure 4c). Almost no movement is observed in either the substrate or the protein side chains. Even though there is only a slight change in the position of metal ion B

Table 1: Summary of Data Collection and Refinement for the All-Oxygen-Mn, All-Oxygen-Zn, dUsG−Mn, and dUsG−Zn Structures

| | structure | | | | |
|---|---|---|---|---|---|
| parameter | all-oxygen-Mn | all-oxygen-Zn | dUsG−Mn | dUsG−Mg | dUsG−Mn (home) |
| PDB accession no. | 2kzm | 2kzz | 2kfn | 2kfz | n/a[a] |
| resolution range (Å) | 20−2.6 | 20−2.25 | 20−2.03 | 20−2.03 | 20−3.2 |
| wavelength (Å) | 0.908 | 1.127 | 0.908 | 0.908 | 1.54 |
| no. of reflections | 289 824 | 173 188 | 422 554 | 422 599 | 86 857 |
| no. of unique reflections, $F > 2\sigma$ | 22 445 [47 722[b]] | 29 618 [60 613] | 50 916 [111 393] | 50 156 [112 871] | 14 513 [28 210] |
| completeness (%) | 89.1 [87.9] | 84.6 [74.7] | 99.0 [93.5] | 98.5 [94.3] | 98.1 [98.0] |
| av $I/\sigma$ | 13.8 [11.9] | 12.8 [10.5] | 16.3 [12.8] | 16.3 [11.7] | 16.8 [11.9] |
| $R_{sym}$[c] | 0.055 [0.049] | 0.068 [0.060] | 0.069 [0.055] | 0.063 [0.052] | 0.102 [0.094] |
| av $I/\sigma$ (highest res shell) | 5.2 [3.5] | 2.2 [1.8] | 3.7 [2.6] | 3.5 [2.4] | 4.5 [3.1] |
| $R_{sym}$ (highest res shell) | 0.211 [0.320] | 0.224 [0.212] | 0.374 [0.348] | 0.332 [0.307] | 0.354 [0.324] |
| no. of protein atoms | 4748 | 4748 | 4748 | 4748 | 4748 |
| no. of waters | 100 | 203 | 316 | 316 | 0 |
| final *R* factor | 0.198 | 0.198 | 0.218 | 0.225 | 0.300[d] |
| final free *R* factor | 0.242 | 0.250 | 0.251 | 0.257 | 0.293 |
| | | rms Deviations | | | |
| bond lengths (Å) | 0.011 | 0.010 | 0.014 | 0.014 | n/a |
| bond angles (deg) | 1.6 | 1.6 | 1.7 | 1.7 | n/a |
| dihedrals (deg) | 23.4 | 23.1 | 23.3 | 23.3 | n/a |
| impropers (deg) | 1.4 | 1.4 | 1.4 | 1.6 | n/a |

[a] These data were not submitted to the PDB because an identical, higher-resolution structure (2kfn) was submitted. These data were used only to calculate an anomalous-difference Fourier map. [b] Numbers in brackets are those obtained when Friedel mates are treated separately to measure anomalous differences (see Materials and Methods). No $\sigma$ cutoff was used. [c]

$$R_{sym} = \sum_{hkl} |\hat{I} - I|_{hkl} \Big/ \sum_{hkl} I_{hkl}$$

where $\hat{I}$ represents the mean intensity value for symmetry- (or Friedel-) equivalent reflections and *hkl* denotes the irreducible set of reflections within the reciprocal-space asymmetric unit. [d] These data were subjected to rigid-body refinement only.

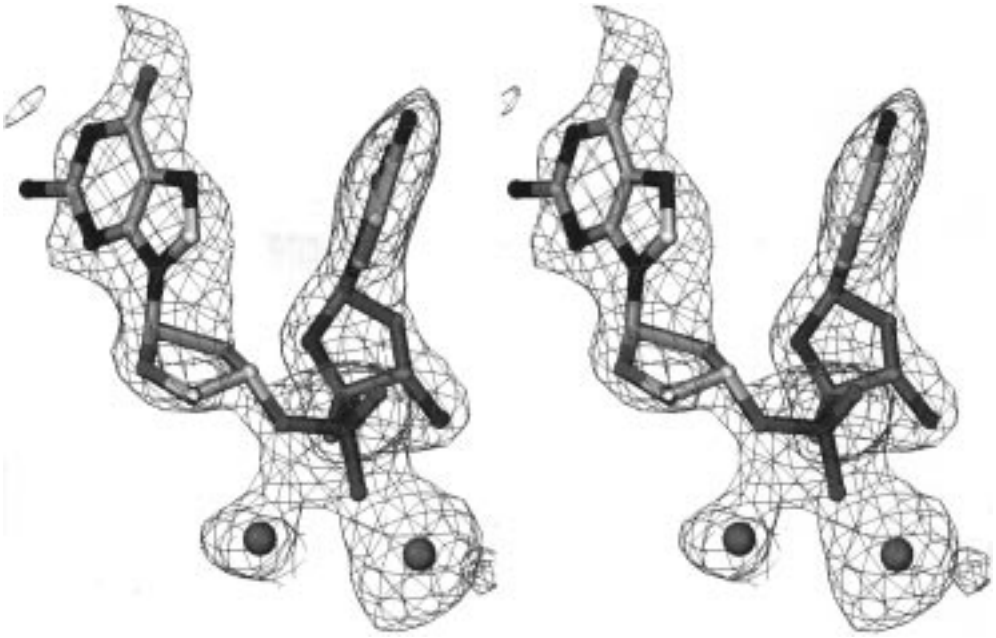

FIGURE 3: Stereoview of the electron density for the substrate and metal ions in the all-oxygen-Mn structure. This 2.6-Å resolution simulated-annealing omit map (*39*), contoured at 1.5$\sigma$, is shown superimposed on the final refined coordinates of the substrate DNA and metal ions in the all-oxygen-Mn structure. All atoms shown had been omitted in the calculation of this map. This figure and all others in this paper featuring electron density were generated using O (*28*).

in the two structures, the electron density at this site in the all-oxygen-Mn structure is consistent with a $Mn^{2+}$ of more disorder and/or less occupancy than the corresponding $Mg^{2+}$ in the all-oxygen-Mg structure (the *B* factor of the $Mn^{2+}$ is twice that of the $Mg^{2+}$).

*All-Oxygen-Zn Structure and Comparison to the All-Oxygen-Mg Structure*. A 2.25-Å resolution structure of an all-oxygen oligonucleotide with $Zn^{2+}$ present as the only divalent cation shows that both metal ion sites are capable of binding $Zn^{2+}$ under these conditions (parts a and b of Figure 5). The structure, which has been refined to an *R* factor of 19.8% and an $R_{free}$ of 25.0%, closely resembles the all-oxygen-Mg structure (*20*; see Figure 5c). The metal ions, side chains, and substrate in the active site are in virtually identical positions in both structures. An anomalous-difference electron-density map confirms the assignment of both metal ions as $Zn^{2+}$ (Figure 5b). The largest difference between the two structures is in metal ion B. Although its

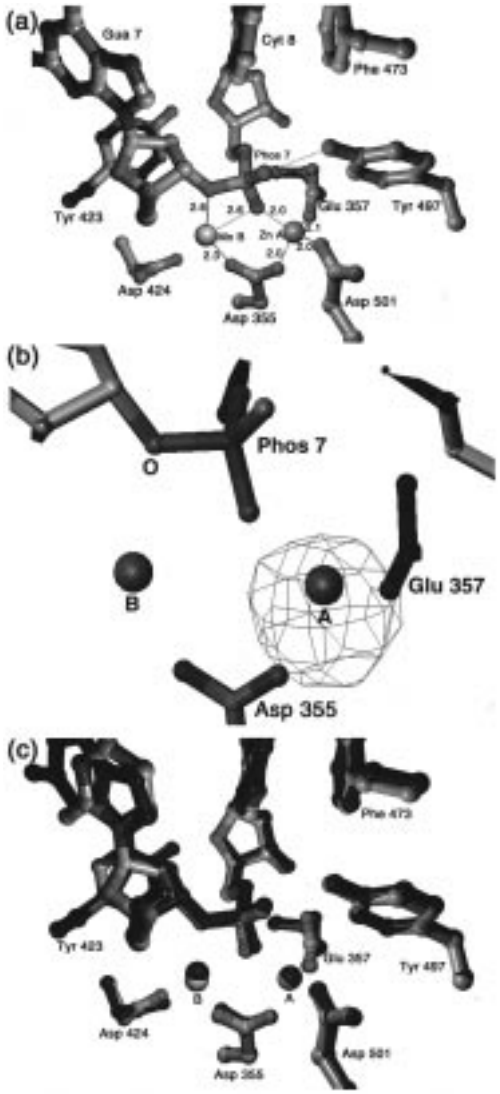


FIGURE 4: Active site of KF exo in the presence of zinc(II) and manganese(II) ions. (a) The active-site configuration of the all-oxygen-Mn structure. Residues with darker carbons belong to the enzyme, and those with lighter carbons represent the DNA substrate. In this and all similar figures, only the 3′-terminal dinucleotide of the DNA is shown. The two metal ions are depicted as spheres. All distances are given in angströms. This and all similar figures were generated using VMD (*38*) and rendered using POV−Ray. (b) Anomalous-difference density for $Zn^{2+}$ in the active site of the all-oxygen-Mn structure. The data were collected at 0.908 Å, a wavelength at which only $Zn^{2+}$ has a significant anomalous signal. The bridging oxygen atom of the all-oxygen substrate is labeled with an "O". Clearly, only metal ion site A contains zinc in this active site. The map is contoured at 4$\sigma$ and is superimposed on the refined coordinates of the all-oxygen-Mn structure. Data between 10.0 and 3.0 Å were used for this and all other anomalous-difference density maps, except where noted. (c) Comparison of the all-oxygen structures in the presence of $Mg^{2+}$ or $Mn^{2+}$. The all-oxygen-Mg structure (*20*) is shown in a lighter shade, and the all-oxygen-Mn structure is darker. Only the $C_\alpha$ atoms from the exonuclease domain of KF (residues 324−540) were used for this and all other superpositions, which were carried out in O (*28*). The rms deviation of the two sets of $C_\alpha$'s was 0.22 Å.

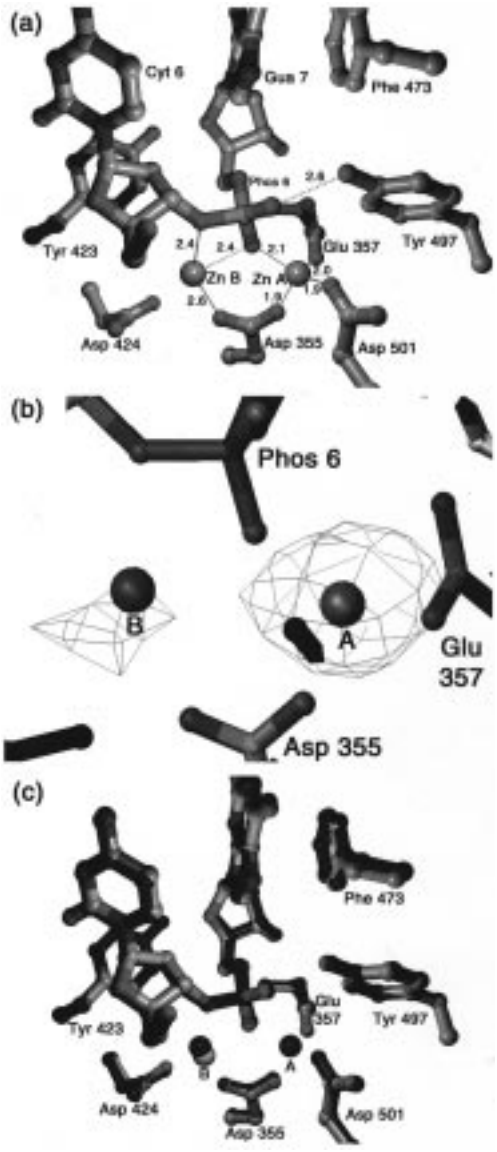


FIGURE 5: KF exo active site in the presence of Zn(II) ion only. (a) The active-site configuration of KF exo in the presence of $Zn^{2+}$. The same shading scheme as that in Figure 4a is used. No water molecule could be identified in inner-sphere contact with metal ion B. (b) An anomalous-difference Fourier map of the active site. The wavelength of the analysis (1.127 Å) was near the anomalous edge for Zn. The contour level of the map is 3$\sigma$. With no other divalent cation present, both metal ion sites are positive for $Zn^{2+}$ binding. (c) A superposition of the all-oxygen-Mg (*20*) and all-oxygen-Zn structures. The all-oxygen-Zn structure is shown in lighter shades, with the all-oxygen-Mg shown darker. The rms deviation between the two structures is 0.19 Å.

position is not significantly different between the two structures (Figure 5c), the *B* factor associated with this metal ion in the all-oxygen-Zn structure is about 3 times that of the metal ion B in the all-oxygen-Mg structure. Therefore, a $Zn^{2+}$ at metal ion site B is more disordered or poorly occupied compared to a $Mg^{2+}$, leading to the abnormally long metal-ion-to-ligand distances (2.0 Å is expected). Perhaps as a consequence of the poor binding of this metal ion, no water molecules can be found near the $Zn^{2+}$ at metal ion site B.

*$Zn^{2+}$/$Mn^{2+}$ 3′PS Structure and Comparison to the All-Oxygen-Mn Structure.* The structure of KF exo in complex with $Zn^{2+}$, $Mn^{2+}$, and a heptamer deoxyoligonucleotide in which the 3′-most phosphodiester linkage was a 3′PS (referred to hereafter as "dUsG", after the last two nucleotides in the heptamer; see Figure 2a) shows that both metal ions bind despite the alteration in the substrate (Figure 6a). This structure (the "dUsG−Mn structure") has been elucidated at 2.03 Å resolution and refined to an *R* factor of 21.8% and

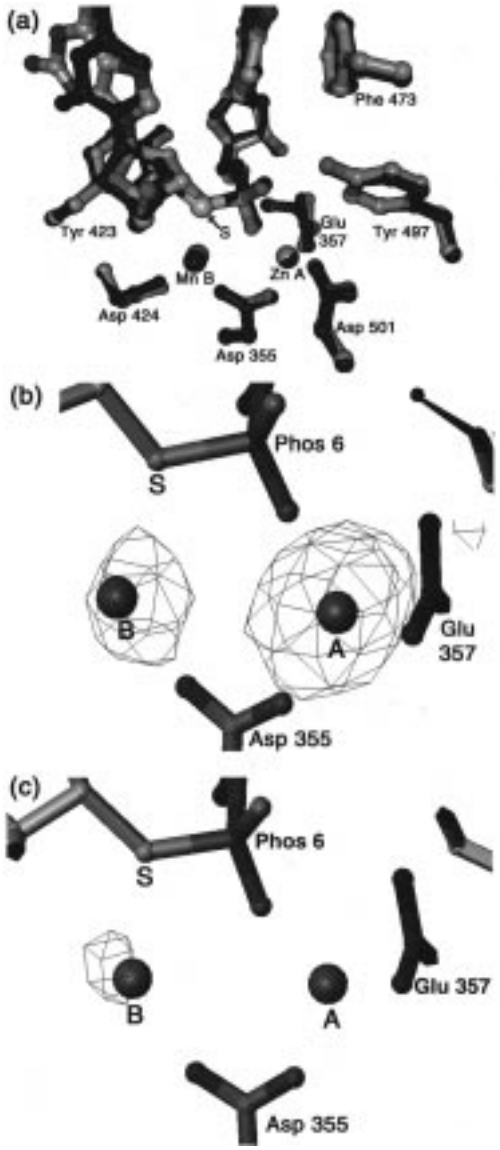


FIGURE 6: Binding properties of dUsG in the presence of manganese(II) and zinc(II) ions. (a) Comparison of the all-oxygen-Mn and the dUsG−Mn structures. The all-oxygen structure is shown in light shades, and the dUsG structure is darker. The bridging sulfur atom of dUsG is highlighted as a large, light-colored sphere. The rms deviation of the two structures is 0.13 Å. (b) Anomalous-difference density for the zinc in the dUsG−Mn structure. The map is contoured at 3$\sigma$. For reference, the bridging sulfur atom of dUsG is labeled with an "S". Because only $Zn^{2+}$ has an anomalous component at the wavelength at which these data were collected (0.908 Å), $Zn^{2+}$ is at least partially occupying both metal ion sites in the presence of dUsG. This and the following map (Figure 4c) are superimposed on the refined coordinates of the dUsG−Mn structure. (c) Anomalous-difference density for manganese in the dUsG−Mn structure. These data were collected at 1.54 Å, a wavelength at which $Mn^{2+}$ has an anomalous signal but $Zn^{2+}$ does not. Clearly, site B is occupied by $Mn^{2+}$ but not site A. The map, contoured at 3$\sigma$, is superimposed on the refined coordinates for the dUsG−Mn structure. Data between 10.0 and 3.2 Å were used.

an $R_{free}$ of 25.1%. The positions of the active-site side chains, when compared to the all-oxygen-Mn structure, are nearly identical. The penultimate nucleotide is somewhat displaced because of the increased lengths of the P−S and S−C covalent bonds, but the position of the phosphorus atom of the scissile phosphate is nearly identical between the two structures. The placement of all other atoms in the 3′-terminal nucleotide also is very similar. Metal ion A is a $Zn^{2+}$, as substantiated by an anomalous-difference electron-density map for data collected near the $Zn^{2+}$ anomalous edge (Figure 6b). A small amount of signal is present in this map for metal ion B, indicating that this site is occupied by $Zn^{2+}$. However, by performing the anomalous-diffraction experiment at a wavelength (1.54 Å) at which $Mn^{2+}$, but not $Zn^{2+}$, has a significant anomalous signal, we demonstrated that $Mn^{2+}$ also occupies this site (Figure 6c). Therefore, under these conditions, $Zn^{2+}$ and $Mn^{2+}$ are competing for binding at metal ion site B. No signal is present in this latter anomalous-difference electron-density map for metal ion A, consistent with its assignment as a $Zn^{2+}$. Metal ion B was modeled as a $Mn^{2+}$ for refinement of the dUsG−Mn structure. As in the all-oxygen-Mn structure, only one water molecule could be found in contact with metal ion B in the dUsG−Mn structure. In comparison to metal ion B of the all-oxygen-Mn structure, the $Mn^{2+}$ is displaced by about 0.4 Å (Figure 6a), a modest difference considering that the rms deviation for the $C_\alpha$'s in KF exo that were used for superposition is 0.13 Å and that the estimated coordinate error for the structures is between 0.25 and 0.3 Å. Overall, the introduction of the sulfur atom into the substrate has only a small effect on the binding of this oligonucleotide and metal ions to the active site of KF exo.

*$Zn^{2+}$/$Mg^{2+}$ 3′PS Structure and Comparison to the All-Oxygen-Zn Structure*. Analysis of a 2.03-Å resolution structure of dUsG bound to KF exo in the presence of $Mg^{2+}$ and $Zn^{2+}$ (the "dUsG−Zn" structure) shows that two zinc(II) ions bind in the KF exo active site under these conditions (parts a and b of Figure 7). This structure has been refined to an $R$ factor of 22.5% and an $R_{free}$ of 25.7%. An anomalous-difference electron-density map shows that both metal ion binding sites contain $Zn^{2+}$ (Figure 7b). Several experiments have been performed to establish whether $Mg^{2+}$ also binds under these conditions (data not shown). Difference electron-density maps calculated with data from crystals which had been soaked in higher or lower concentrations of $Mg^{2+}$ reveal no changes at the active site. Lowering [$Zn^{2+}$] by 10-fold has also been attempted. Under these conditions, electron-density maps show that no metal ion binds at site B. We therefore conclude that when a 3′PS is bound at the KF exo active site, $Mg^{2+}$ does not bind at metal ion site B in a manner that is amenable to crystallographic characterization.

Because the dUsG−Zn structure appears to bind $Zn^{2+}$ only, the most appropriate structure for comparison is the all-oxygen-$Zn^{2+}$ structure (Figure 7a). This comparison shows only small changes in the positions of the metal ions and protein side chains. As in the dUsG−Mn structure, the modified substrate binds similarly to the all-oxygen oligonucleotide. Metal ion B in the dUsG−Zn structure is shifted away from the all-oxygen-Zn position by about 1 Å. This movement is probably significant considering the small error in the superposition of the two structures (0.19-Å rms deviation) and the estimated coordinate errors (between 0.25 and 0.3 Å).

## DISCUSSION

*3′ Phosphorothiolates as Substrates for KF Exonuclease*. An important goal of the present structural study has been to answer the following question: why is the KF exo-catalyzed hydrolysis of a 3′PS more efficient in the presence

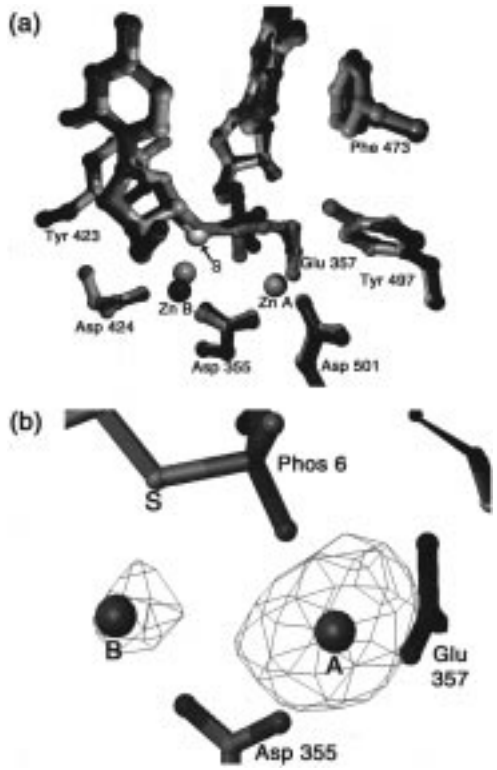


FIGURE 7: Binding properties of dUsG in the presence of magnesium(II) and zinc(II) ions. (a) Comparison of the all-oxygen-Zn and the dUsG−Zn structures. The all-oxygen structure is shown in a lighter shade, and the dUsG−Zn structure is darker. The bridging sulfur atom of dUsG is again highlighted as a large, light-colored sphere. (b) Anomalous-difference density for zinc in the active site of the dUsG−Zn structure. Again using the wavelength at which only $Zn^{2+}$ has a signal (0.908 Å), both metal ions are highlighted. The contour level of this map is 3$\sigma$.

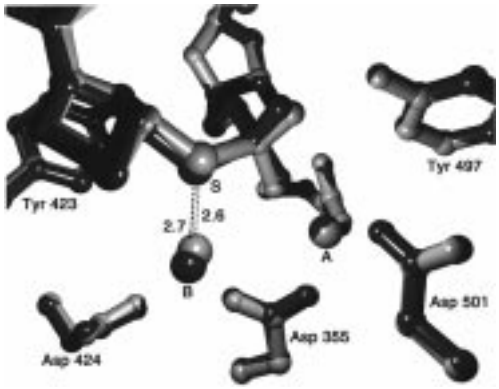


FIGURE 8: Comparison of the dUsG−Mn and dUsG−Zn active sites. Shown in the dark shade is the dUsG−Zn structure, with the lighter shade depicting the dUsG−Mn structure. The structures are nearly identical. The bridging sulfur atom is marked with an "S", and the distances between the metal ions and this leaving group are shown in angströms.

of $Mn^{2+}$ than $Mg^{2+}$? This issue has been kinetically addressed recently (*15*), and it was suggested that the difference lies in the superior ability of $Mn^{2+}$ at metal ion site B to stabilize the negative charge that builds up on the leaving sulfur atom in the transition state. Our crystallographic experiments point to an additional explanation based on a property of thiophilic cations that is expressed in both the ground state and transition state of the reaction: enzyme-bound 3′PSs allow only thiophilic metal ions to bind at metal ion site B. In the two structures which feature KF complexed with 3′PS (KF·3′PS), $Mn^{2+}$, a thiophilic cation, occupies site B (Figure 6c), and $Mg^{2+}$ does not. Site-directed mutagenesis studies have shown that elimination of metal ion B decreases the enzyme activity of KF exo $10^5$-fold (*10*, *31*). We thus conclude that it is the poor binding of $Mg^{2+}$ at metal ion site B in the KF·3′PS complex that accounts for the inefficiency of this metal ion in supporting the hydrolysis of a 3′PS bond. Furthermore, the fact that $Mn^{2+}$ can bind relatively well at site B in the KF·3′PS complex explains its facility in promoting the reaction on the altered substrate. It appears, therefore, that the answer to the above question is that $Mn^{2+}$ is better able to bind at metal ion site B in the presence of 3′PSs and thus supports their hydrolysis much more efficiently than $Mg^{2+}$.

The fact that $Zn^{2+}$ can bind at metal ion site B in the dUsG−Mn and dUsG−Zn structures (Figures 6b and 7b) suggests that $Zn^{2+}$, like $Mn^{2+}$, should be able to support the KF exo-catalyzed hydrolysis of 3′PS substrates. A comparison of the two structures (Figure 8) shows that the sulfur-substituted substrate does not deviate significantly in position, conformation, occupancy, or disorder regardless of whether $Mn^{2+}$ and $Zn^{2+}$ or $Zn^{2+}$ alone occupies metal ion site B. The B metal ions are in different positions in the two structures, but their distances to the bridging sulfur atom are conserved. Furthermore, it has been observed that when KF crystals are soaked in solutions containing a 3′PS and $Zn^{2+}$ at pH 7.0, electron density for product dNMP can be observed in the active site (*30*), suggesting that the exonucleolytic reaction has taken place in the crystal. Taken together, these facts strongly suggest that KF exo can hydrolyze 3′PS substrates in the presence of $Zn^{2+}$. It would be informative to explore crystallographically and biochemically the effect of $Zn^{2+}$ and other thiophilic metal ions (e.g., $Cd^{2+}$) on the action of KF exo on a 3′PS.

It is unexpected that the catalytic efficiency of KF exo on a 3′PS is still 600-fold depressed relative to all-oxygen substrates in the presence of $Mn^{2+}$ (*15*; Figure 2b), because $Mn^{2+}$ binds $O^-$ with about the same affinity as it binds $S^-$ (*16*) and sulfur is better able to harbor negative charge, which should make it a better leaving group (*32*, *33*). Weaker binding of the 3′PS and/or metal ion B could contribute to the 600-fold effect. Additionally, the degree of perturbation to the active site of the dUsG−Mn structure relative to the all-oxygen-Mn structure is reminiscent of the changes which occur when the $R_p$ diastereomer of phosphorothioate DNA binds to this active site (*20*). Because the activity of KF exo on the $R_p$ diastereomer is similarly slowed (15−100 times slower $V_o$ compared to all-oxygen; *20*, *22*), the changes in the dUsG−Mn active site could fully explain the observed inhibition. However, the geometry of the binding site for metal ion B might also contribute. The enzyme and substrate create an octahedral liganding environment for this cation (*2*, *20*). On the other hand, thioanions, owing to their large size, prefer to exist in a tetrahedral coordination sphere around metals the size of $Zn^{2+}$, $Mn^{2+}$, or $Mg^{2+}$ (*34*). Therefore, the reduction in catalytic efficiency may be attributable to some extent to the steric crowding of ligands around the metal ion.

*3′ Phosphorothiolates as Substrates for Other Nucleases.* These studies provide insight into the observation that ribozymes prefer thiophilic metal ions as cofactors in the

hydrolysis of bridging sulfur substrates (*13*, *18*, *19*). As noted above, the metal ion site B of the KF·3′PS complex may bind thiophilic metal ions but not $Mg^{2+}$. These observed cation preferences are in accord with the known liganding propensities of sulfur (*17*). They therefore demonstrate that the 3′-bridging atom of the scissile phosphate is an integral part of the ligation environment of metal ion B, despite its distance from the cation (2.6−2.8 Å) and previous expectations of a repulsive or weak interaction between these two atoms (*35*). If an analogous catalytically essential metal ion binding site is present in the ribozyme systems, the bridging sulfur ligand of the substrate may bias the site toward binding thiophilic cations. Alternatively, a tightly bound $Mg^{2+}$ resident at such a site could negatively affect the ability of a bridging sulfur substrate to bind.

*Binding of DNA and Metal Ions to KF Exo*. The results presented in this study yield a number of new insights into the binding of ssDNA to KF exo. Several substrate ssDNAs of various lengths and sequences have been investigated using our crystallographic methodology (vide infra; see also ref *20*). Neither of these factors has caused significant changes in the binding behavior of these substrates to KF exo (Figures 4c and 5c). The most striking feature of metal ion binding in these experiments is that all of the B metal ions studied ($Mn^{2+}$ or $Zn^{2+}$) exhibited significant disorder (and/or low occupancy). This is surprising in the case of the all-oxygen structures, given that with all-oxygen DNAs (i) $Mg^{2+}$ is well-ordered at site B (*20*), (ii) KF is more catalytically efficient with $Mn^{2+}$ than with $Mg^{2+}$ (*15*), and (iii) $Zn^{2+}$ increases the rate of the KF exo-catalyzed reaction (*36*). It is possible that the high salt conditions of the crystal (2.8 M ammonium sulfate) disrupt the ability of these cations to bind to the active site of KF exo. In the dUsG structures, the B metal ions are slightly displaced from their all-oxygen positions and have high *B* factors. The bulky sulfur atom of the 3′PS, which is in close proximity to metal ion B, could contribute to the poor binding, in addition to the factors enumerated above for metal ion A binding.

## CONCLUSIONS

The results presented in this X-ray crystallographic study of the binding of 3′-phosphorothiolates to the 3′-5′ exonuclease active site of the Klenow fragment reveal several important facts about these nuclease-resistant compounds. We have shown that $Mn^{2+}$, but not $Mg^{2+}$, can bind to the crystalline KF·3′PS complex at the catalytically essential metal ion site B. These results explain the in vitro observation that $Mn^{2+}$ is much more efficient than $Mg^{2+}$ in supporting the hydrolysis of 3′PSs by KF (*15*). There is also evidence that $Zn^{2+}$ can act as a cofactor in this reaction. These studies provide a general framework for understanding how 3′PSs resist the action of metal-ion-dependent nucleases. Further, our results establish the binding characteristics of $Zn^{2+}$ and $Mn^{2+}$ at metal ion site B and indicate that the substitution of the 3′-bridging oxygen atom of the substrate's scissile phosphate by a sulfur has only subtle consequences for the positioning of the DNA in this active site.

## ACKNOWLEDGMENT

The authors thank Catherine Joyce for her gift of wild-type Klenow fragment and helpful discussions, Nigel Grindley, Paul Sigler, and Fritz Eckstein for critical evaluations of the manuscript (in thesis form), Jessica Curley for providing data and helpful discussions, and Laura Silvian, Nenad Ban, Yousif Shamoo, Steven Bellon, and Daniel Kaplan for assistance with data collection. We also thank Kathryn Aschheim for essential assistance in the revision of this manuscript. Some of the research in this paper was conducted at the Cornell High Energy Synchrotron Source (CHESS), which is supported by the National Science Foundation under Award DMR-9311772, using the Macromolecular Diffraction at CHESS (MacCHESS) facility, which is supported by award RR-01646 from the National Institutes of Health. In addition, some of the research was carried out at the National Synchrotron Light Source, Brookhaven National Laboratory, which is supported by the U.S. Department of Energy, Division of Materials Sciences and Division of Chemical Sciences.

## REFERENCES

1. Freemont, P. S., Friedman, J. M., Beese, L. S., Sanderson, M. R., and Steitz, T. A. (1988) *Proc. Natl. Acad. Sci. U.S.A. 85*, 8924−8928.
2. Beese, L. S., and Steitz, T. A. (1991) *EMBO J. 10*, 25−33.
3. Steitz, T. A. (1993) *Curr. Opin. Struct. Biol. 3*, 31−38.
4. Pelletier, H., Sawaya, M. R., Kumar, A., Wilson, S. H., and Kraut, J. (1994) *Science 264*, 1891−1903.
5. Doublié, S., Tabor, S., Long, A. M., Richardson, C. C., and Ellenberger, T. (1998) *Nature 391*, 251−258.
6. Brautigam, C. A., and Steitz, T. A. (1998) *Curr. Opin. Struct. Biol. 8*, 54−63.
7. Kim, E. E., and Wyckoff, H. W. (1991) *J. Mol. Biol. 218*, 449−464.
8. Davies, J. F., Hostomska, Z., Hostomsky, Z., Jordan, S. R., and Matthews, D. A. (1991) *Science 252*, 88−95.
9. Steitz, T. A., and Steitz, J. A. (1993) *Proc. Natl. Acad. Sci. U.S.A. 90*, 6498−6502.
10. Derbyshire, V., Freemont, P. S., Sanderson, M. R., Beese, L., Friedman, J. M., Joyce, C. M., and Steitz, T. A. (1988) *Science 240*, 199−201.
11. Cosstick, R., and Vyle, J. S. (1990) *Nucleic Acids Res. 8*, 2295−2300.
12. Vyle, J. S., Conolly, B. A., Kemp, D., and Cosstick, R. (1992) *Biochemistry 31*, 3012−3018.
13. Piccirilli, J. A., Vyle, J. S., Caruthers, M. H., and Cech, T. R. (1993) *Nature 361*, 85−88.
14. Sun, S., Yoshida, A., and Piccirilli, J. A. (1997) *RNA 3*, 1352−1363.
15. Curley, J. F., Joyce, C. M., and Piccirilli, J. A. (1997) *J. Am. Chem. Soc. 119*, 12691−12692.
16. Pecoraro, V. L., Hermes, J. D., and Cleland, W. W. (1984) *Biochemistry 23*, 5262−5271.
17. Sigel, R. K. O., Song, B., and Sigel, H. (1997) *J. Am. Chem. Soc. 119*, 744−755.
18. Weinstein, L. B., Jones, B. C. N. M., Cosstick, R., and Cech, T. R. (1997) *Nature 388*, 805−808.
19. Sontheimer, E. J., Sun, S., and Piccirilli, J. A. (1997) *Nature 388*, 801−805.
20. Brautigam, C. A., and Steitz, T. A. (1998) *J. Mol. Biol. 277*, 363−377.
21. Kunkel, T. A., Eckstein, F., Mildvan, A. S., Koplitz, R. M., and Loeb, L. A. (1981) *Proc. Natl. Acad. Sci. U.S.A. 78*, 6734−6738.
22. Gupta, A. P., Benkovic, P. A., and Benkovic, S. J. (1984) *Nucleic Acids Res. 12*, 5897−5911.
23. Brick, P., Ollis, D., and Steitz, T. A. (1983) *J. Mol. Biol. 166*, 453−456.
24. Szebenyi, D. M. E., Arvia, A., Ealick, S., Laluppa, J. M., and Nielsen, C. (1997) *J. Synchrotron Radiat. 4*, 128−135.
25. Otwinowski, Z., and Minor, W. (1997) *Methods Enzymol. 276*, 307−325.

26. Brünger, A. T. (1992). *X-PLOR*, version 3.1, Yale University Press, New Haven, CT.
27. Read, R. J. (1986) *Acta Crystallogr*., *Sect*. *A 42*, 140−149.
28. Jones, T. A., Zou, J.-Y., Cowan, S. W., and Kjeldgaard, M. (1991) *Acta Crystallogr*., *Sect*. *A 47*, 110−119.
29. Collaborative Computational Project, Number 4. (1994) *Acta Crystallogr*., *Sect*. *D 50*, 760−763.
30. Brautigam, C. A. (1997) Ph.D. Thesis, Yale University, New Haven, CT.
31. Derbyshire, V., Grindley, N. D. F., and Joyce, C. M. (1991) *EMBO J*. *10*, 17−24.
32. Kuimelis, R. G., and McLaughlin, L. W. (1995) *Nucleic Acids Res*. *23*, 4753−4760.
33. Frey, P. A. (1989) *Adv*. *Enzymol*. *Relat*. *Areas Mol*. *Biol*. *62*, 119−201.
34. Kaim, W., and Schwederski, B. (1994) *Bioinorganic Chemistry: Inorganic Elements in the Chemistry of Life*. *An Introduction and Guide*, John Wiley & Sons, Chichester, U.K.
35. Narlikar, G. J., Gopalakrishnan, V., McConnell, T. S., Usman, N., and Herschlag, D. (1995) *Proc*. *Natl*. *Acad*. *Sci*. *U.S.A*. *92*, 3668−3672.
36. Derbyshire, S. V. (1991) Ph.D. Thesis, Yale University, New Haven, CT.
37. Derbyshire, V., Pinsonneault, J. K., and Joyce, C. M. (1995) *Methods Enzymol*. *262*, 363−385.
38. Humphrey, W., Dalke, A., and Schulten, K. (1996) *J*. *Mol*. *Graphics 14*, 33−38.
39. Hodel, A., Kim, S.-H., and Brünger, A. T. (1992) *Acta Crystallogr*., *Sect*. *A 48*, 851−859.

BI981537G